Volume 7
Number 15
7 August 2023
Pages 3473–3728

Sustainable Energy & Fuels

Interdisciplinary research for the development of sustainable energy technologies

rsc.li/sustainable-energy

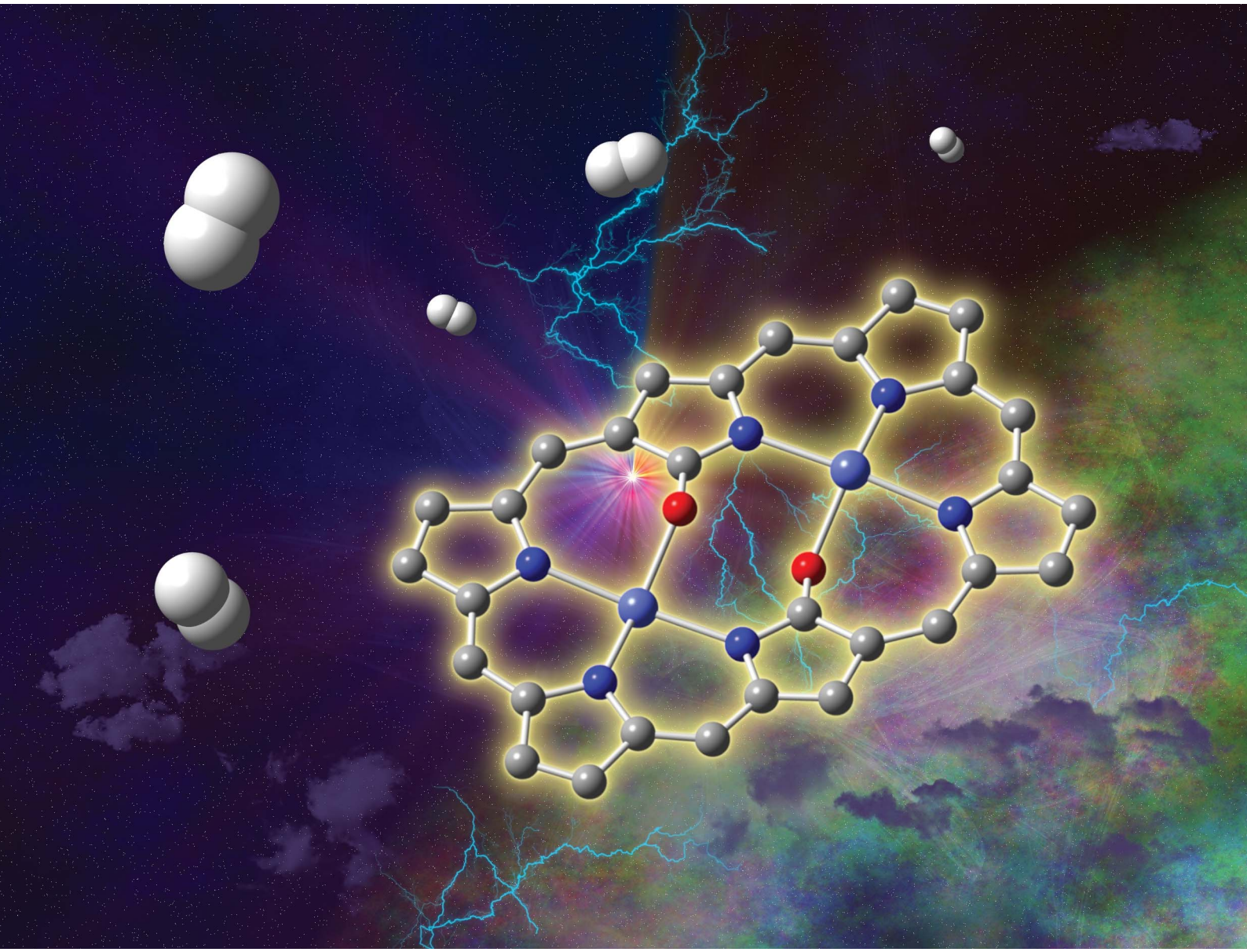

ISSN 2398-4902

ROYAL SOCIETY OF CHEMISTRY

PAPER

Takashi Nakazono, Tohru Wada *et al.*
Electrochemical hydrogen evolution reaction catalysed by a dinuclear cobalt complex with doubly N-confused hexaphyrin

Sustainable Energy & Fuels

ROYAL SOCIETY OF CHEMISTRY

PAPER

View Article Online
View Journal | View Issue

Cite this: *Sustainable Energy Fuels*, 2023, 7, 3603

Electrochemical hydrogen evolution reaction catalysed by a dinuclear cobalt complex with doubly N-confused hexaphyrin†

Risa Takada,[a] Takashi Nakazono, *[b] Taiyo Nishimura,[a] Takuya Shiga,[c] Masayuki Nihei,[c] Yusuke Yamada [bd] and Tohru Wada *[a]

Received 27th March 2023
Accepted 26th May 2023

DOI: 10.1039/d3se00403a

rsc.li/sustainable-energy

In this study, we discovered the high catalytic activity of a dinuclear cobalt complex, Co_2DNCH, supported by a doubly N-confused hexaphyrin (DNCH), a kind of ring-expanded porphyrin, for the electrochemical hydrogen evolution reaction. Co_2DNCH catalysed electrochemical hydrogen evolution reaction with onset-overpotential $\eta = 0.45$ V in water at pH 7.0, and with $\eta = 0.54$ V and turnover frequency TOF = 2.27×10^4 s^{-1} in DMF containing Et_3NHCl as a proton source. Furthermore, electrochemical measurements and density functional theory calculations elucidated that the large π-conjugated system of the DNCH ligand enables two-electron reduction centred on DNCH and hydrogen evolution at a relatively positive potential.

Introduction

Hydrogen is a non-polluting fuel with a high energy density per unit weight. It produces only water as a product following combustion and generation of electricity by a fuel cell.[1,2] Hydrogen production is currently based on reforming natural gas and water–gas shift reactions, accompanied by CO_2 generation. Electrochemical water reduction can be an alternative for clean hydrogen production without CO_2 emissions by combination with highly effective solar photovoltaic generation.[3] Although platinum is well known as an extremely active catalyst for the hydrogen evolution reaction (HER), its deposit in the earth's crust is small.[4,5]

Therefore, the development of an HER catalyst composed of earth-abundant metals is required to realise a society based on hydrogen energy. In nature, hydrogenase containing a [FeFe] or [FeNi]-dinuclear complex as a reaction centre effectively catalyses hydrogen evolution and oxidation reactions.[6,7] First-row transition metal complexes have the potential to be efficient HER catalysts. In fact, many complexes have been reported as molecular HER catalysts.[8–13] In most of the previously proposed reaction pathways, HER proceeds through the hydride complex as an active species, which is formed by the reaction of an intermediate, which contains a low-valent metal ion with a vacant coordination site with a proton. The ligand stabilising such an intermediate is necessary for HER catalysts with first-row transition metal ions.

Porphyrin is a typical macrocyclic ligand whose metal complexes serve as a highly active and durable HER catalysts.[14] Moore *et al.* previously reported that dinuclear copper(II) porphyrin, in which two macrocyclic copper(II) porphyrin molecules are doubly fused at the *meso*-β position, exhibits a remarkably high turnover rate (TOF = 2.0×10^6 s^{-1}) for electrochemical HER.[15] Furthermore, the triply fused Cu porphyrin reported by Sarkar *et al.* generates H_2 with an overpotential of 320 mV lower than the non-fused monomer.[16] These interesting reports inspired us to investigate dinuclear complexes supported by macrocyclic ligands.

Herein, we focused on dinuclear cobalt complexes with doubly N-confused hexaphyrin (1.1.1.1.1) (**Co_2DNCH**, Fig. 1), which is a ring-expanded porphyrin. Cobalt porphyrin complexes have long been studied as highly active in

[a]*Department of Chemistry, College of Science, Rikkyo University, 3-34-1 Nishi-Ikebukuro, Toshima-ku, Tokyo 171-8501, Japan. E-mail: twada@rikkyo.ac.jp*
[b]*Research Center for Artificial Photosynthesis (ReCAP), Osaka Metropolitan University, 3-3-138 Sugimoto, Sumiyoshi-ku, Osaka 558-8585, Japan. E-mail: nakazono@omu.ac.jp*
[c]*Department of Chemistry, Faculty of Pure and Applied Sciences, University of Tsukuba, Tennodai 1-1-1, Tsukuba 305-8571, Ibaraki, Japan*
[d]*Department of Chemistry and Bioengineering, Graduate School of Engineering, Osaka Metropolitan University, 3-3-138 Sugimoto, Sumiyoshi-ku, Osaka 558-8585, Japan*
† Electronic supplementary information (ESI) available. See DOI: https://doi.org/10.1039/d3se00403a

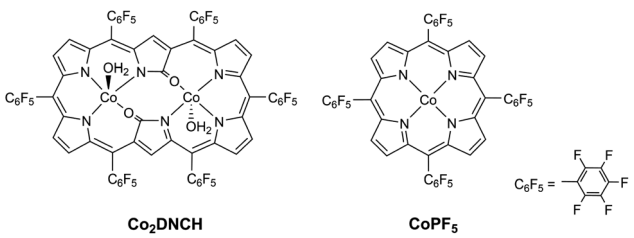

Fig. 1 Structure of Co_2DNCH (left) and $CoPF_5$ (right).

electrochemical HER in both water and organic solvents.[17–20] **Co_2DNCH** was firstly synthesised by Furuta, Kim and Osuka,[21] however, the catalytic activity for HER had never been reported. We have reported **Co_2DNCH** shows high catalytic activity for photochemical water oxidation for the first time.[22] A free base DNCH (H_4DNCH) with a Hückel aromatic 26π-conjugated system is capable of multi-electron reduction at more positive potential than porphyrins with 18π-conjugated systems.[23,24] It can accommodate two first-row transition-metal ions. **Co_2DNCH** is expected to be a significant HER catalyst due to these characteristics.

In this paper, we report for the first time that **Co_2DNCH** serves as a highly efficient HER catalyst. The HER catalytic activity of **Co_2DNCH** was studied in water and in *N*,*N*-dimethylformamide (DMF). Moreover, the redox properties and HER catalytic activity of **Co_2DNCH** were compared with those of **$CoPF_5$** (PF_5 = *meso*-tetrakis(pentafluorophenyl)porphyrinato, Fig. 1) with the same C_6F_5 substituents. The catalytic reaction mechanism is discussed based on the results of electrochemical, spectroelectrochemical and density functional theory (DFT) measurements.

Results and discussion

The HER catalytic activity of **Co_2DNCH** and **$CoPF_5$** in water was investigated by linear sweep voltammetry (LSV, Fig. 2). LSVs were performed using a glassy carbon electrode modified with each catalyst and a multi-walled carbon nanotube (MW-CNT; Preparation method of the modified electrode is described in the Experimental section), because the catalyst is insoluble in water. The LSVs showed a large cathodic current derived from HER at pH 7.0 (Fig. 2). The onset potential of hydrogen evolution (E_{HER}) of **Co_2DNCH** was −1.1 V (*vs.* SCE), which was 350 mV more positive than that of **$CoPF_5$** (E_{HER} = −1.45 V). E_{HER} of **Co_2DNCH** decreased with increasing pH of the solution, where the slopes were −59 mV pH^{-1} (Fig. S1 and S2†). The onset-overpotentials of **Co_2DNCH** and **$CoPF_5$** were η = 0.45 and 0.80 V, respectively. After LSV using the **Co_2DCNCH**-modified electrode, the electrode was washed with acetone. The LSV using the electrode was almost consistent with that using a glassy carbon electrode modified with only MW-CNT. Thus, the catalyst was not decomposed and functioned as a molecular catalyst (Fig. S3 and S4†). The controlled-potential electrolysis at −1.1 V using **Co_2DNCH** or **$CoPF_5$** modified electrodes in phosphate buffer (pH 7) evolved hydrogen (Fig. S5†) with turnover numbers (TON) = 703 for **Co_2DNCH** and TON = 125 for **$CoPF_5$** in 50 min. Both of the Faraday efficiencies were more than 98%.

The LSVs using the modified electrodes showed only a broad reduction wave derived from the redox reaction of the complexes at −0.5 V. To investigate the detailed redox behaviour of **Co_2DNCH**, we performed cyclic voltammetry (CV) of the complexes in DMF (Fig. 3 and Table S1†). The CV of **Co_2DNCH** showed three reversible waves in $E_{1/2}$ = −0.47, −0.80 and −1.49 V, and an irreversible redox wave at E_{pc} = −1.65 V in the potential range between 0 V and −2.00 V. Alternatively, two redox waves were observed in the CV of **$CoPF_5$** at $E_{1/2}$ = −0.6 and −1.59 V under the same conditions. These indicate that the two metal centres and the large π-conjugated system of **Co_2DNCH** enable the four-electron storage at more positive potentials than −2.00 V.

Spectroelectrochemical measurements of **Co_2DNCH** were performed to assign redox waves (Fig. 4). In the UV-vis spectrum of **Co_2DNCH** in DMF, the Soret-like band was observed at 614 nm, and the Q-like bands were observed at 933 and 1054 nm.[25] When the **Co_2DNCH** was reduced at −0.6 V, the absorbance of the Soret-like band at 614 nm decreased, and a new absorption band appeared at 580 nm. Meanwhile, the Q-like bands at 933 and 1054 nm disappeared, and a broad absorption band around 850–1050 nm appeared. This new broad band is consistent with that of π radical species previously reported for DNCH analogues,[26,27] indicating that the first reduction of **Co_2DNCH** is assigned to the DNCH-centred reduction to form $[Co_2(DNCH^{\bullet-})]^-$. Further electrolysis at −1.0 V caused the disappearance of the broad absorption band around 850–1050 nm. Thus, the second reduction reaction is also most likely to be the DNCH-based reaction.

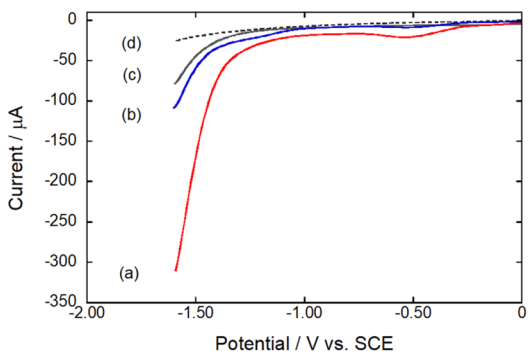

Fig. 2 LSVs using the complex-modified glassy carbon electrode in a 0.10 M phosphate buffer solution (pH 7.0). Working electrode: glassy carbon (0.071 cm^2) modified with **Co_2DNCH** and MW-CNT (a), **$CoPF_5$** and MW-CNT (b), MW-CNT (c), bare glassy carbon (d), counter electrode: Pt wire, reference electrode: SCE, scan rate: 0.10 V s^{-1}, temp: 295 K.

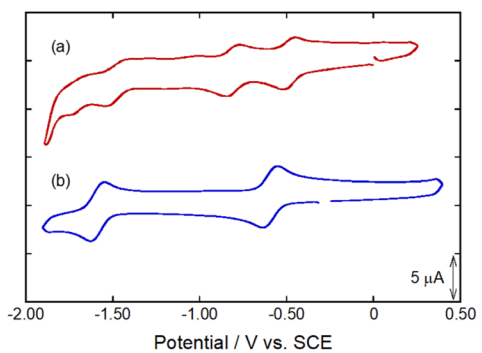

Fig. 3 CVs of DMF solutions containing **Co_2DNCH** (a) and **$CoPF_5$** (b). Working electrode: glassy carbon (0.071 cm^2), counter electrode: Pt, reference electrode: $Ag/AgNO_3$, complex: 0.25 mM, electrolyte: *n*-Bu_4NClO_4 (100 mM), scan rate: 0.10 V s^{-1}, temp: 295 K. All potentials were converted to voltages *vs.* SCE.

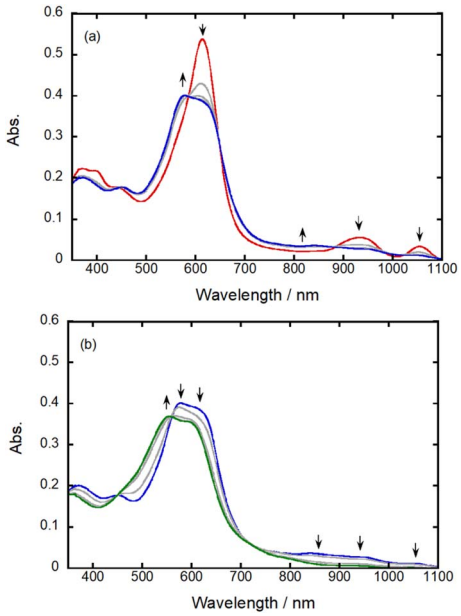

Fig. 4 UV-vis absorption spectra of the DMF solutions of **Co$_2$DNCH** (0.14 mM) before (red in (a)) and after controlled-potential electrolysis at −0.6 V (blue in (a) and (b)) and −1.0 V (green in (c)). Optical path length: 0.5 mm, working electrode: Pt mesh, counter electrode: Pt wire, reference electrode: Ag/AgNO$_3$, electrolyte: *n*-Bu$_4$NClO$_4$ (100 mM). All potentials were converted to voltages *vs.* SCE.

In previous studies, the spin state of **Co$_2$DNCH** was expected to be $S = 1/2$ (low spin state) per cobalt ion; however, no experimental evidence has been reported to support this hypothesis.[28] The temperature dependence of the magnetic susceptibility for **Co$_2$DNCH** (Fig. S6†) was measured to determine the spin state of **Co$_2$DNCH**. The $\chi_M T$ value of **Co$_2$DNCH** is 5.58 emu mol^{-1} K at room temperature, which decreases upon cooling (0.43 emu mol^{-1} K at 1.8 K). The $\chi_M T$ value at room temperature is close to those expected for magnetically isolated two Co^{2+} ions with an $S = 3/2$ state.[29] Therefore, we assigned the spin state, and the oxidation number of the cobalt ions in **Co$_2$DNCH** was $S = 3/2$ (HS) per Co^{2+} ion. The decrease of $\chi_M T$ values at lower temperatures suggests antiferromagnetic interactions between two Co^{2+} ions. Co^{2+} porphyrines, which are the analogue of **Co$_2$DNCH**, are generally low spin and insensitive to axial ligands because of small electron exchange energy in high-spin Co^{2+} as compared to that in high-spin Fe^{2+}.[30] High-spin state of **Co$_2$DNCH** would be arising from the weak ligand field and distorted pyramidal structure composed of the O atoms of the DNCH ring and axial OH_2.

To theoretically support this assignment, we performed the DFT calculation at the uB3LYP/Lanl2DZ (for Co) and 6-31G* (for the other elements) levels of theory with a simplified model of **Co$_2$DNCH** and its reduced forms in which all pentafluorophenyl groups were replaced by H atoms and aqua ligands were omitted to reduce computational cost (see the DFT calculation section of ESI†). The bond lengths and angles of the optimised **Co$_2$DNCH** structure are comparable to those of the previously reported single-crystal structure (Fig. S7, S8, and Table S2†). The most stable spin state of **Co$_2$DNCH** as the ground state was estimated to be septet ($2S + 1 = 7$) (Table S3†), which is consistent with the result of the magnetic susceptibility measurement. The spin densities of **Co$_2$DNCH** and its reduced forms of one and two electrons were visualised (Fig. S9†). The spin density on the two Co ions and DNCH ligand of the one-electron reduced state remains and increases, respectively, compared with those of the initial state, strongly supporting the assignment of the first reduction reaction to the ligand-based one (Table S4†). The octet is the most stable spin state of the one-electron reduced form, which results from two high-spin Co^{2+} ions ($S = 3/2$ per a Co^{2+}) and DNCH radical ($S = 1/2$). The spin density on the DNCH of the two-electron-reduced form has almost disappeared.

Furthermore, the septet state is more stable than the nonet state by 25.8 kcal mol^{-1}. These results of DFT calculations support the claim that consecutive two-step ligand-based reductions of **Co$_2$DNCH** provide $[Co_2(DNCH^{2-})]^{2-}$, in which two electrons make the spin pair in DNCH. A similar redox behaviour of H_4DNCH was reported by Furuta *et al.*[24]

To investigate the catalytic activities of HER in organic solutions and these reaction mechanisms, CVs of **Co$_2$DNCH** and **CoPF$_5$** in the presence of proton sources were performed in DMF. Influences of pK_a of proton sources on the catalytic current and redox waves in CV provide important information to elucidate the reaction mechanism.[31] We used triethylammonium chloride (Et_3NHCl, $pK_a^{DMF} = 9.2$), acetic acid (AcOH, $pK_a^{DMF} = 13.5$) and phenol (PhOH, $pK_a^{DMF} = 18.0$) as proton sources.[32,33] When 2.0, 5.0 and 10.0 equiv. of Et_3NHCl as the strongest acid in the three were gradually added to the DMF solution of **Co$_2$DNCH**, the catalytic current arising from HER increased at a negative potential greater than −1.2 V, which was between the second and third reduction potentials of **Co$_2$DNCH** in the absence of a proton source (Fig. 5a). The overpotential was determined by eqn (1) and (2) based on CVs.[34]

$$\text{Overpotential} = \left| E_{H^+} - \frac{E_{cat}}{2} \right| \quad (1)$$

$$E_{H^+} = E^{\circ}_{H^+} - 0.059 \times pK_a^{DMF} \quad (2)$$

where $E^{\circ}_{H^+}$ is the equilibrium electrode potential of HER in DMF, $E_{cat/2}$ is the potential at half of the catalytic current (i_{cat}), and pK_a^{DMF} is pK_a in DMF of the proton source used. $E^{\circ}_{H^+} = -736$ V *vs.* SCE, which was calculated from $E^{\circ}_{H^+}$ determined by Mayer and co-workers (−0.662 V *vs.* $Fc^{+/0}$),[35] and $pK_a^{DMF} = 9.2$ for Et_3NHCl[33] were used for eqn (2). Overpotential of **Co$_2$DNCH** was calculated to be 0.54 V. In the case that the electron transfer between catalyst molecules and electrodes is sufficiently fast, the substrate concentration is sufficiently high, and the catalytic current is limited only by the chemical reaction in solution, the pseudo-first-order rate constant k_{obs}, which corresponds to the TOF of HER catalyst, can be calculated using eqn (3).[36,37]

$$\frac{i_{cat}}{i_p} = \frac{2}{0.4463}\sqrt{\frac{k_{obs}RT}{F\nu}} \quad (3)$$

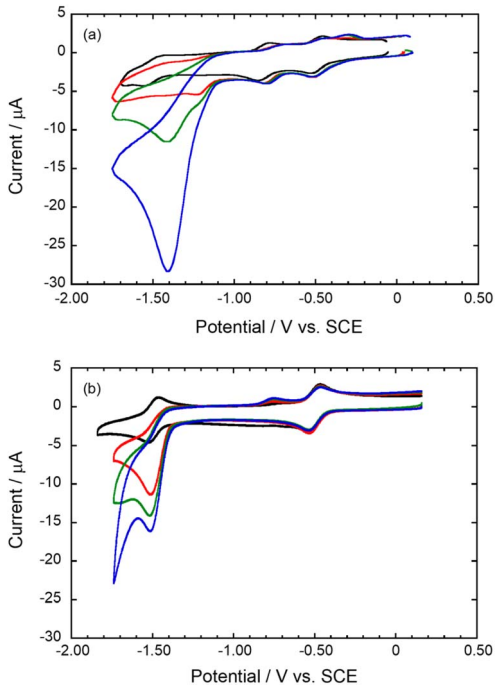

Fig. 5 CVs of the DMF solutions of Co_2DNCH (a) and $CoPF_5$ (b) in the absence (black) and presence of triethylammonium chloride: 2.0 (red), 5.0 (green) and 10 equiv. (blue). Working electrode: glassy carbon (0.071 cm^2), counter electrode: Pt, reference electrode: $Ag/AgNO_3$, complex: 0.25 mM, electrolyte: n-Bu_4NClO_4 (100 mM), scan rate: 0.10 V s^{-1}, temp: 295 K. All potentials were converted to voltages *vs.* SCE.

where i_{cat} is the peak value of catalytic current in the presence of 200 equiv. of Et_3NHCl, i_p is the peak current of the third reduction wave of **Co_2DNCH** in the absence of a proton source, R is the ideal gas constant, T is the temperature of CV measurements (295 K), F is the Faraday constant and v is the scan rate of CVs. In both cases, i_{cat}/i_p values are in direct proportion to $v^{-1/2}$ (Fig. S10 and S11†). We determined that the TOF of **Co_2DNCH** was 2.27×10^4 s^{-1} (Fig. S12†) based on the slope of i_{cat}/i_p at −1.4 V. for **Co_2DNCH**. On the other hand, CV of **$CoPF_5$** in the presence of Et_3NHCl also showed a large cathodic current with shoulder peack bellow −1.4 V (Fig. 5b). The potential of shoulder peak is consistent to that of the second redox wave of **$CoPF_5$** in the absence of Et_4NHCl; therefore, this irreversible wave is assignable to the EC reaction of $[\mathbf{CoPF_5}]^-$ to form $[CoHPF_5]^-$. However, we could not determine TOF of **$CoPF_6$** because catalytic current of HER catalyzed by **$CoPF_6$** was overlapped with the current derived from hydrogen evolution on the glassy carbon electrode. It is clear that **Co_2DNCH** catalyses HER with lower overpotential than **$CoPF_5$**. Moore reported that the Cu-fused porphyrin complex, which has a large conjugated system and two metal centres like **Co_2DNCH**, also shows markedly high TOF of 2×10^6 s^{-1} in DMSO in the presence of trifluoroacetic acid (TFA) as a proton source.[15] These phenomena suggest that the large π-conjugated system of ring-expanded and extended porphyrins accommodating multi-metal centres is advantageous for the HER catalysis.

The addition of Et_3NHCl to the solution slightly affected the first and second redox waves of **Co_2DNCH**, and the potential of the catalytic wave shifted significantly more positively than the third redox wave in the absence of Et_3NHCl. Protonation rate accompanying reduction of the complex may be slow compared with the scan rate of CV. We, therefore, performed the CVs of **Co_2DNCH** at slow scan rate (5 mV s^{-1}) (Fig. S13a†). An irreversible reduction wave appeared at −0.29 V with the addition of Et_3NHCl, suggesting protonation of **Co_2DNCH**. When CV was performed at a faster scan rate (100 mV s^{-1}), the same reduction wave was observed at the same potential, although the current was smaller (Fig. S14†). Thus, the first protonation process is expected to be slow. This new reduction wave is not consistent with that of H_4DNCH, nor is it due to the formation of a new species by the coordination of Cl^- ions (Fig. S15†). The second and third waves at −0.42 and −0.75 V were reversible. Catalytic current was increased from −1.2 V, which unaffected by decrease of scan rate. These observations suggest the $[CoCoH(DNCH)]^{3-}$ reacts with Et_3NHCl to form H_2 and HER proceeds *via* (EC)EE(EC) process. When PhOH was used as a proton source, the reversibility of first and second waves at −0.42 and −0.75 V maintained and a new one-electron reduction wave was observed at −1.2 V with a small catalytic current at −1.6 V (Fig. S16a†). This CV changes mean that three-electron reduced form react with a proton to form $[CoCoH(DNCH)]^{2-}$. $[Co(CoH)(DNCH)]^{2-}$ did not react with PhOH as a weak acid, and the four-electron reduced form $[Co(CoH)(DNCH)]^{3-}$ yielded hydrogen. The shoulder waves at −1.2 and −1.3 V in the CV of **Co_2DNCH** containing 200 equiv. of AcOH would evoke the existence of dihydride species, but there is no clear evidence to support this hypothesis (Fig. S16b†). When PhOH and AcOH was used as proton sources, decreases of scan rates resulted in no significant changes of CVs.

To investigate the third reduction process that occurs at −1.2 V in the presence of AcOH, the kinetic isotope effect (KIE) was calculated using eqn (4).[38]

$$\frac{k_{cat,H^+}}{k_{cat,D^+}} = \left(\frac{i_{cat,AcOH}}{i_{cat,AcOD}}\right)^2 \quad (4)$$

When the shoulder peak of catalytic current at −1.2 V was adopted in the presence of AcOH or AcOD as i_{cat} (Fig. S17†), KIE was 1.2, indicating that this process involves protonation. Therefore, $[Co_2(DNCH^{2-})]^{2-}$ is reduced at −1.2 V followed by protonation to give $[Co(CoH)(DNCH)]^{2-}$, which reacts with H^+ to produce H_2. The relatively small KIE value (1.2) suggests that a part of $[Co(CoH)DNCH]^{2-}$ generated at −1.2 V produces H_2 because the HER of $[Co(CoH)DNCH]^{2-}$ with AcOH is slow. In contrast, reactions at −1.9 V showed relatively large KIE values: 2.7 for AcOH/AcOD because the hydrogen evolution rates of the reactions of $[Co(CoH)(DNCH)]^{3-}$ with AcOH are much faster than those of $[Co(CoH)(DNCH)]^{2-}$.

Based on the observations above, we propose the HER mechanism of **Co_2DNCH** in organic solution (Scheme 1). When Et_3NHCl was used as the strongest acid in the three, the first reduction of **Co_2DNCH** followed by protonation forms the

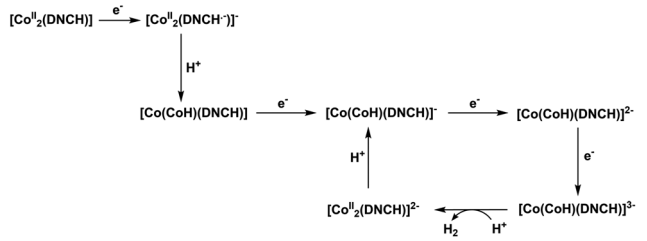

Scheme 1 Proposed mechanism of HER catalysed by Co_2DNCH in the presence of Et_3NHCl as a proton source.

hydride intermediate [CoCoH(DNCH)]. Stepwise two-electron reduction of the hydride intermediate give the reaction active species $[CoCoH(DNCH)]^{2-}$. Following one-electron reduction to form $[CoCoH(DNCH)]^{3-}$ as a reaction active species, which reacts with a proton to produce H_2. In the case of AcOH and PhOH used, three-electron reduced form, $[Co_2(DNCH)]^{3-}$, is protonated to give $[CoCoH(DNCH)]^{2-}$, which slowly reacts with AcOH as a relatively strong acid. Further reduction of $[Co(CoH)(DNCH)]^{2-}$ to $[Co(CoH)(DNCH)]^{3-}$ causes fast hydrogen evolution even with PhOH (Scheme S1†). In the case of water, the second reduction of **Co_2DNCH** may be a CPET process due to the large mobility of the proton in water.

Co_2DNCH has a large π-conjugated system of DNCH allowing the ligand to accommodate two electrons. In the case of relatively acidic conditions, multi-electron reduction of the hydride intermediate provides highly active species of HER. Furthermore, the high basicity of the resultant two-electron-reduced form of **Co_2DNCH** enables protonation and further reduction to generate the catalytic active species at relatively positive potential even when relatively week acid is used. On the other hand, **$CoPF_5$** requires a more negative potential for the reduction accompanying a protonation and hydrogen evolution. Therefore, the large π-conjugated system of DNCH is advantageous to HER.

Experimental

Synthesis

All solvents and reagents were of the highest quality available and were used as received. **Co_2DNCH** was synthesised according to literature[21] and characterized by ESI-MS and elemental analysis. **$CoPF_5$** was prepared using the literature method.[39]

Instrumentation

Electrochemical measurements. All electrochemical measurements were recorded on ECstat-301 (EC Frontier Co. Ltd). Electrochemical measurements of **Co_2DNCH** and **$CoPF_5$** in aqueous solutions were performed using a three-electrode system consisting of a modified glassy carbon working electrode, a platinum wire counter electrode, and an SCE reference electrode. Complex catalyst-modified working electrodes were prepared by casting 1 μL DMF solution containing 1.2 g L^{-1} multi-walled carbon nanotubes (MW-CNT: 35 μg cm^{-2}) and 0.21 mM **Co_2DNCH** or **$CoPF_5$** (3.0 nmol cm^{-2}) on 0.071 cm^2 glassy carbon and drying up at room temperature. Electrochemical measurements of **Co_2DNCH** and **$CoPF_5$** in DMF solution were performed using a three-electrode system consisting of a glassy carbon working electrode, a platinum wire counter electrode and a reference $Ag/AgNO_3$ electrode. Tetra(*n*-butyl) ammonium perchlorate was used as a supporting electrolyte of the DMF solutions.

UV-vis measurements. UV-vis absorption spectra were recorded using a UV1800 spectrophotometer (Shimadzu co). All sample solutions were maintained at 295 K during the spectrophotometric measurements.

DFT calculations. All quantum chemical calculations were done with DFT calculation using the Gaussian 16W programme package (Gaussian Inc).[40] Calculation was done using uB3LYP functional and basis sets of 6-31G* for C, H, O, N and LANL2DZ for Co with PCM model with DMF.[41–43] Calculation was performed using a simplified model in which the pentafluorophenyl groups were substituted with H, and aqua ligands were omitted to reduce the computational cost (see the DFT calculation section of ESI†).

Magnetic measurements. Magnetic susceptibility data were collected under an applied magnetic field of 1 T using a Quantum Design MPMS-5XL SQUID magnetometer. Magnetic data were corrected for the diamagnetism of the sample holder and for the diamagnetism of the sample using Pascal's constants.

Conclusions

In this paper, we have reported the catalytic activity of **Co_2DNCH** for electrochemical hydrogen evolution reaction (HER) in water and DMF. **Co_2DNCH** catalysed HER with $\eta = 0.45$ V in water and with $\eta = 0.54$ V and TOF = 2.27×10^4 s^{-1} in DMF. The catalytic activity of **Co_2DNCH** is much higher than that of **$CoPF_5$**. CVs and DFT calculations show that the stepwise two-electron reduction occurring at DNCH promotes protonation of the Co centre of **Co_2DNCH** even when relatively week acid is used. Therefore, the large π-conjugation system of DNCH is highly useful for electrochemical HER catalysts. This study provided new insights into the research regions of electrochemical HER and ring-expanded porphyrin complexes.

Conflicts of interest

There were no conflicts to declare.

Acknowledgements

This work was supported by JSPS Early Career Scientists (Grant 20K15303), Grant-in-Aid for Scientific Research (C) (Grant 18K05158) and Grant-in-Aid for Scientific Research (B) (Grant 22H01871). This work was also supported by JSPS KAKENHI (Grant 20H05116) in Scientific Research on Innovative Areas 'Innovations for Light-Energy Conversion (I4LEC)', JGC-S Scholarship Foundation, and ENEOS Tonengeneral Research/Development Encouragement & Scholarship Foundation. The authors would like to applicate for Prof. Masahiro Yamanaka of Rikkyo Univ. to support DFT study.

Notes and references

1 A. Kudo and Y. Miseki, *Chem. Soc. Rev.*, 2009, **38**, 253–278.
2 M. Chatenet, B. G. Pollet, D. R. Dekel, F. Dionigi, J. Deseure, P. Millet, R. D. Braatz, M. Z. Bazant, M. Eikerling, I. Staffell, P. Balcombe, Y. Shao-Horn and H. Schafer, *Chem. Soc. Rev.*, 2022, **51**, 4583–4762.
3 X. Zou and Y. Zhang, *Chem. Soc. Rev.*, 2015, **44**, 5148–5180.
4 B. Ruqia and S. I. Choi, *ChemSusChem*, 2018, **11**, 2643–2653.
5 C. Li and J. B. Baek, *ACS Omega*, 2020, **5**, 31–40.
6 J. C. Fontecilla-Camps, P. Amara, C. Cavazza, Y. Nicolet and A. Volbeda, *Nature*, 2009, **460**, 814–822.
7 B. E. Barton and T. B. Rauchfuss, *J. Am. Chem. Soc.*, 2010, **132**, 14877–14885.
8 D. Brazzolotto, M. Gennari, N. Queyriaux, T. R. Simmons, J. Pécaut, S. Demeshko, F. Meyer, M. Orio, V. Artero and C. Duboc, *Nat. Chem.*, 2016, **8**, 1054–1060.
9 M. L. Helm, M. P. Stewart, R. M. Bullock, M. R. DuBois and D. L. DuBois, *Science*, 2011, **333**, 863–866.
10 K. E. Dalle, J. Warnan, J. J. Leung, B. Reuillard, I. S. Karmel and E. Reisner, *Chem. Rev.*, 2019, **119**, 2752–2875.
11 C. Baffert, V. Artero and M. Fontecave, *Inorg. Chem.*, 2007, **46**, 1817–1824.
12 F. Gloaguen, J. D. Lawrence and T. B. Rauchfuss, *J. Am. Chem. Soc.*, 2001, **123**, 9476–9477.
13 K. Kawano, K. Yamauchi and K. Sakai, *Chem. Commun.*, 2014, **50**, 9872–9875.
14 B. B. Beyene and C. H. Hung, *Coord. Chem. Rev.*, 2020, **410**, 213234.
15 D. Khusnutdinova, B. L. Wadsworth, M. Flores, A. M. Beiler, E. A. Reyes Cruz, Y. Zenkov and G. F. Moore, *ACS Catal.*, 2018, **8**, 9888–9898.
16 S. Chandra, A. S. Hazari, Q. Song, D. Hunger, N. I. Neuman, J. van Slageren, E. Klemm and B. Sarkar, *ChemSusChem*, 2023, **16**, e202201146.
17 R. M. Kellett and T. G. Spiro, *Inorg. Chem.*, 1985, **24**, 2373–2377.
18 J. G. Kleingardner, B. Kandemir and K. L. Bren, *J. Am. Chem. Soc.*, 2014, **136**, 4–7.
19 H. M. Castro-Cruz and N. A. Macías-Ruvalcaba, *Coord. Chem. Rev.*, 2022, **458**, 214430.
20 M. Natali, A. Luisa, E. Iengo and F. Scandola, *Chem. Commun.*, 2014, **50**, 1842–1844.
21 M. Suzuki, M. C. Yoon, D. Y. Kim, J. H. Kwon, H. Furuta, D. Kim and A. Osuka, *Chem.–Eur. J.*, 2006, **12**, 1754–1759.
22 T. Nakazono and T. Wada, *Inorg. Chem.*, 2020, **60**, 1284–1288.
23 H. Lei, Y. Wang, Q. Zhang and R. Cao, *J. Porphyrins Phthalocyanines*, 2020, **24**, 1361–1371.
24 I. Mayer, K. Nakamura, A. Srinivasan, H. Furuta, H. E. Toma and K. Araki, *J. Porphyrins Phthalocyanines*, 2005, **9**, 813–820.
25 J. H. Kwon, T. K. Ahn, M.-C. Yoon, D. Y. Kim, M. K. Koh, D. Kim, H. Furuta, M. Suzuki and A. Osuka, *J. Phys. Chem. B*, 2006, **110**, 11683–11690.
26 T. Koide, G. Kashiwazaki, M. Suzuki, K. Furukawa, M.-C. Yoon, S. Cho, D. Kim and A. Osuka, *Angew. Chem., Int. Ed.*, 2008, **47**, 9661–9665.
27 K. Yamasumi, K. Nishimura, Y. Hisamune, Y. Nagae, T. Uchiyama, K. Kamitani, T. Hirai, M. Nishibori, S. Mori and S. Karasawa, *Chem.–Eur. J.*, 2017, **23**, 15322–15326.
28 G. Sun, E. Lei, X.-S. Liu, X.-X. Duan and C.-G. Liu, *J. Mol. Model.*, 2018, **24**, 1–9.
29 Y. Rechkemmer, F. D. Breitgoff, M. Van Der Meer, M. Atanasov, M. Hakl, M. Orlita, P. Neugebauer, F. Neese, B. Sarkar and J. Van Slageren, *Nat. Commun.*, 2016, **7**, 1–8.
30 V. V. Smirnov, E. K. Woller and S. G. DiMagno, *Inorg. Chem.*, 1998, **37**, 4971–4978.
31 N. Queyriaux, D. Sun, J. Fize, J. Pecaut, M. J. Field, M. Chavarot-Kerlidou and V. Artero, *J. Am. Chem. Soc.*, 2020, **142**, 274–282.
32 K. Izutsu, *Acid-Base Dissociation Constants in Dipolar Aprotic Solvents*, Blackwell Scientific Publication, 1990.
33 V. Fourmond, P. A. Jacques, M. Fontecave and V. Artero, *Inorg. Chem.*, 2010, **49**, 10338–10347.
34 A. M. Appel and M. L. Helm, *ACS Catal.*, 2014, **4**, 630–633.
35 M. L. Pegis, J. A. S. Roberts, D. J. Wasylenko, E. A. Mader, A. M. Appel and J. M. Mayer, *Inorg. Chem.*, 2015, **54**, 11883–11888.
36 E. S. Rountree, B. D. McCarthy, T. T. Eisenhart and J. L. Dempsey, *Inorg. Chem.*, 2014, **53**, 9983–10002.
37 M. Okamura, M. Kondo, R. Kuga, Y. Kurashige, T. Yanai, S. Hayami, V. K. Praneeth, M. Yoshida, K. Yoneda, S. Kawata and S. Masaoka, *Nature*, 2016, **530**, 465–468.
38 F. Yu, D. Poole III, S. Mathew, N. Yan, J. Hessels, N. Orth, I. Ivanovic-Burmazovic and J. N. H. Reek, *Angew. Chem., Int. Ed.*, 2018, **57**, 11247–11251.
39 S. A. Jannuzzi, E. G. de Arruda, F. A. Lima, M. A. Ribeiro, C. Brinatti and A. L. Formiga, *ChemistrySelect*, 2016, **1**, 2235–2243.
40 M. J. Frisch, G. W. Trucks, H. B. Schlegel, G. E. Scuseria, M. A. Robb, J. R. Cheeseman, G. Scalmani, V. Barone, G. A. Petersson, H. Nakatsuji, X. Li, M. Caricato, A. V. Marenich, J. Bloino, B. G. Janesko, R. Gomperts, B. Mennucci, H. P. Hratchian, J. V. Ortiz, A. F. Izmaylov, J. L. Sonnenberg, D. Williams-Young, F. Ding, F. Lipparini, F. Egidi, J. Goings, B. Peng, A. Petrone, T. Henderson, D. Ranasinghe, V. G. Zakrzewski, J. Gao, N. Rega, G. Zheng, W. Liang, M. Hada, M. Ehara, K. Toyota, R. Fukuda, J. Hasegawa, M. Ishida, T. Nakajima, Y. Honda, O. Kitao, H. Nakai, T. Vreven, K. Throssell, J. A. Montgomery Jr., J. E. Peralta, F. Ogliaro, M. J. Bearpark, J. J. Heyd, E. N. Brothers, K. N. Kudin, V. N. Staroverov, T. A. Keith, R. Kobayashi, J. Normand, K. Raghavachari, A. P. Rendell, J. C. Burant, S. S. Iyengar, J. Tomasi, M. Cossi, J. M. Millam, M. Klene, C. Adamo, R. Cammi, J. W. Ochterski, R. L. Martin, K. Morokuma, O. Farkas, J. B. Foresman and D. J. Fox, *Gaussian 16, Revision B.01*, Gaussian, Inc., Wallingford CT.
41 P. J. Hay and W. R. Wadt, *J. Chem. Phys.*, 1985, **82**, 270–283.
42 W. R. Wadt and P. J. Hay, *J. Chem. Phys.*, 1985, **82**, 284–298.
43 P. J. Hay and W. R. Wadt, *J. Chem. Phys.*, 1985, **82**, 299–310.

